arXiv:1003.0333v4 [cond-mat.mes-hall] 5 Mar 2010

First-principles calculations of the magnetic properties of (Cd,Mn)Te nanocrystals

C. Echeverría-Arrondo,[1,2,3] J. Pérez-Conde,[1] and A. Ayuela[3,2]

[1]*Departamento de Física, Universidad Pública de Navarra, E-31006, Pamplona, Spain*
[2]*Donostia International Physics Center (DIPC), E-20018, San Sebastián/Donostia, Spain*
[3]*Departamento de Física de Materiales, Facultad de Químicas, Centro de Física de Materiales CSIC-UPV/EHU, E-20018, San Sebastián/Donostia, Spain*

(Dated: March 5, 2010)

We investigate the electronic and magnetic properties of Mn-doped CdTe nanocrystals (NCs) with ~ 2 nm in diameter which can be experimentally synthesized with Mn atoms inside. Using the density functional theory, we consider two doping cases: NCs containing one or two Mn impurities. Although the Mn d peaks carry five up electrons in the dot, the local magnetic moment on the Mn site is 4.65 μ_B. It is smaller than 5 μ_B because of the sp-d hybridization between the localized $3d$ electrons of the Mn atoms and the s- and p-type valence states of the host compound. The sp-d hybridization induces small magnetic moments on the Mn nearest-neighbor Te sites, antiparallel to Mn moment affecting the p-type valence states of the undoped dot, as usual for a kinetic mediated exchange magnetic coupling. Furthermore, we calculate the parameters standing for the sp-d exchange interactions: Conduction $N_0\alpha$ and valence $N_0\beta$ are close to the experimental bulk values when the Mn impurities occupy bulk-like NCs' central positions, and they tend to zero close to the surface. This behavior is further explained by an analysis of valence band-edge states showing that symmetry breaking splits the states and in consequence reduces the exchange. For two Mn atoms in several positions, the valence edge states show a further departure from an interpretation based in a perturbative treatment. We also calculate the d-d exchange interactions $|J^{dd}|$ between Mn spins. The largest $|J^{dd}|$ value is also for Mn atoms on bulk-like central sites; in comparison with the experimental d-d exchange constant in bulk $Cd_{0.95}Mn_{0.05}Te$ it is four times smaller.

I. INTRODUCTION

The recent progress in chemical synthesis, computational capabilities and scanning-probe techniques has permitted a detailed understanding of semiconductor nanocrystals (NCs) – also known as nanoparticles, clusters, crystallites or quantum dots (QDs). Their properties which depend on size[1–5] and shape[3] have overimposed effects due to quantum confinement. For instance, when the QD radius is smaller than the Bohr radius of exciton, quantum-confinement effects appear, such as the blue shift of gaps and the discretization of energy spectra[1–6]. The gap properties can also be tuned intentionally with doping[6–13]. Recently, much effort has focused on II-VI semiconductor NCs doped with magnetic impurities such as Mn, which is the topic of this work. The Mn doping is motivated by diluted magnetic semiconductors (DMSs). These compounds are bulk semiconductors doped with transition-metal impurities such as Cr, Mn, Fe and Co at low concentrations. DMSs are current research materials in spintronics, integrated in novel magnetoelectronic devices such as spin-LEDs[14]. Their remarkable magnetic and magneto-optical properties result from the strong sp-d exchange interactions between band carriers and Mn ions[10]. These interactions yield giant band-edge splittings at low temperature (about 100 meV)[15]. In particular, little is known theoretically about exchange in NCs made of II-VI DMSs doped with Mn.

DMS NCs of type II-VI doped with Mn have been successfully synthesized and characterized during the last fifteen years. These works found at zero field, or low fields, contradictory results for the Zeeman splitting. In comparison with bulks, several authors have shown a reduction of the excitonic Zeeman splitting in Mn-doped CdS[16], CdSe[17] and CdTe[10,18,19] NCs. Other works revealed no enhancement of the excitonic Zeeman splitting in Co-doped ZnO, ZnSe and CdS QDs[20] in comparison with their bulk values. Magnetic circular dichroism and optical experiments with Mn-doped ZnSe NCs revealed a value for the same splitting of 28 meV, much larger than in bulk ZnSe:Mn[11].

The Zeeman splittings are due on one hand to the confinement-enhanced sp-d hybridization between the occupied Mn $3d$ orbitals and the sp-type valence states of the host compound; and on the other hand to the crystal field experienced by Mn impurities, which is significantly different nearer the NC surface than in bulk[21]. Experimentally, several authors found that Mn atoms are embedded in ZnSe NCs[11], and even a single Mn impurity is inside CdTe nanocrystals[22]. Theoretically, enhanced splittings are obtained in ZnSe:Mn NCs within the effective mass approximation[23] with a single Mn sitting at the center. However, there is little theoretical information about exchange interactions and splittings for CdTe:Mn NCs, and even less with Mn off-center. We also note that the DMS NCs can hold inside several Mn impurities.

In the present work we study Mn-doped CdTe NCs of spherical shape with the density functional theory. In section II we give a brief account of the theorical framework and numerical details. The host compound is a well-known wide-gap semiconductor of type II-VI, and manganese is a widely-used dopant, known for activating photo- and electroluminescence, and also for contributing to efficient luminescence centers ($3d$ electrons)[24]. Sev-

eral authors have previously calculated the properties of bulk II-VI CdTe doped with Mn[25–27]. We consider two doping situations: NCs including one and two Mn impurities, which substitute for one or two Cd atoms in the zinc blende lattice, respectively. In section III the results concerning NCs with a single Mn impurity are given. The results for NC with two impurities are described in section IV. We calculate the total ground-state energy of the QD, for several positions of impurities within the crystal and the magnetic state. Moreover, we obtain the *sp-d* and *d-d* exchange constants[25] as a function of the Mn locations: $N_0\alpha$ and $N_0\beta$ stand for the exchange interactions between the Mn local moments and the *s*- and *p*-type band-edge states of the host CdTe; J^{dd} parametrizes the exchange interaction between two Mn spins. Finally, we sum up the main findings and concluding remarks in section V. The system described here may provide further understanding of solid-state qubits, since it permits to detect and manipulate a single spin[22]. In addition it could show magnetic and magneto-optical properties, such as fast recombination and high luminescence efficiency[8].

II. COMPUTATIONAL DETAILS

The many-body problem for the electrons around the nuclei is solved based on the density functional theory (DFT), using the Kohn-Sham equations. The valence electrons move in the external potential created by the nuclei and the core electrons. The electronic states of the studied NCs are obtained from the projector augmented-wave method as implemented in the VASP code[28–30]. To account for the *sp-d* hybridization[25] the ten $3d$ spin-orbitals of Mn impurities are included in our calculations. Within DFT, our approach for the exchange-correlation is defined with the generalized-gradient approximation (GGA) of Perdew, Burke and Ernzerhof[31]. However, the interactions among the $3d$ electrons of Mn impurities in the GGA approximation are only partially described, since they are strongly localized. Thus, we use the so-called GGA+U scheme and introduce in the calculations two common correction parameters, U and J[33]. For Mn atoms in CdTe bulk, $U = 6.2$ eV and $J = 0.86$ eV. They are considered to correct the Coulomb (U) and exchange (J) interactions among the $3d$ electrons at Mn sites[32,33]. We have checked that with the U values of Refs. 32 and 33 for Mn, the density of states are very similar, especially the d peak corresponding to Mn is nearly at the same energy. This peak is below the *p*-type part of the CdTe valence band. We have chosen the recent U value in Ref. 33 because it calculated MnTe bulk where Mn is surrounded by Te. Additionally, tests on bulk MnTe with the same lattice constant of Ref. 33 show nearly the same band structures when using LSDA or GGA and the same U value.

The input parameters for the VASP calculations are determined in a preliminary work for two model bulk systems, CdTe and F-MnTe (zinc blende). For several lattice constants we fitted the ground-state energies to the Murnaghan's equation of state, which depends on the unit cell volume. The equilibrium lattice constants of bulks CdTe and F-MnTe are $a_{CdTe} = 6.63$ Å and $a_{F-MnTe} = 6.38$ Å. The cut-off energy in the plane wave basis set is 350 eV; this is the shared cut-off to converge the ground-state energies of both CdTe and F-MnTe bulks within meV.

The studied NCs are spherical about 17 Å in diameter centered on a cation site (Cd). The crystal structure is zinc blende, which has tetrahedral (T_d) symmetry around the atoms. These QDs are passivated since otherwise the surface dangling bonds would introduce surface states in the near-gap spectrum. Organic ligands are commonly used to passivate NCs, but we want to center on the intrinsic properties of NCs[34]. For the sake of simplicity we resort to the simplest passivation agent: a pseudo-hydrogen atom (H^*). The fictitious H^* is characterized by fractional electronic charge and by a proton with the same charge but positive. Every Cd ($5s^2$) dangling bond includes 2/4 unpaired electrons, so it is bound to a pseudohydrogen atom with a fictitious charge of 6/4 *e*. Similarly, every Te dangling bond ($5s^2\ 5p^4$) is bound to a pseudohydrogen atom with an electronic charge of 2/4 *e*. When the pseudohydrogen atoms H^* are included the NCs have 107 atoms in total: 19 Cd, 28 Te and 60 H^*. We dope them with one or two Mn impurities depending on the studied case.

We use the supercell approximation to deal with a single nanocrystal. We place the NC at the center of a large cubic unit cell and take the Γ point. Then we have converged the ground-state energies of two small model NCs ($CdTe_4H^*_{12}$ and $MnTe_4H^*_{12}$) versus the supercell size within meVs. We consider that this separation between walls is valid for larger NCs. The input distances between nearest-neighbor atoms are taken from those in Cd-Te bulk. We have $d_{Cd-Te} = (\sqrt{3}/4)a_{CdTe} = 2.87$ Å and take $d_{Mn-Te} = d_{Cd-Te}$. The atomic structures are relaxed until the forces on each atom are smaller than 0.02 eV/ Å.

III. NANOCRYSTALS WITH A SINGLE MN IMPURITY

A. Energetics and Geometry for Mn Atom in Different Positions

We study NCs doped with a unique Mn impurity substituting a single Cd atom. The NC geometry is plotted in Fig. 1 (a). The cation sites of the NC are distributed in three sets, and labeled as "I" for the sphere center, "II" for other inner positions and "III" for outside positions. The substitutional energy is the energy difference ΔE_1 of the following reaction:

$$\text{CdTe NC} + \text{Mn}^{+2} \longrightarrow \text{CdTe:Mn NC} + \text{Cd}^{+2}. \quad (1)$$

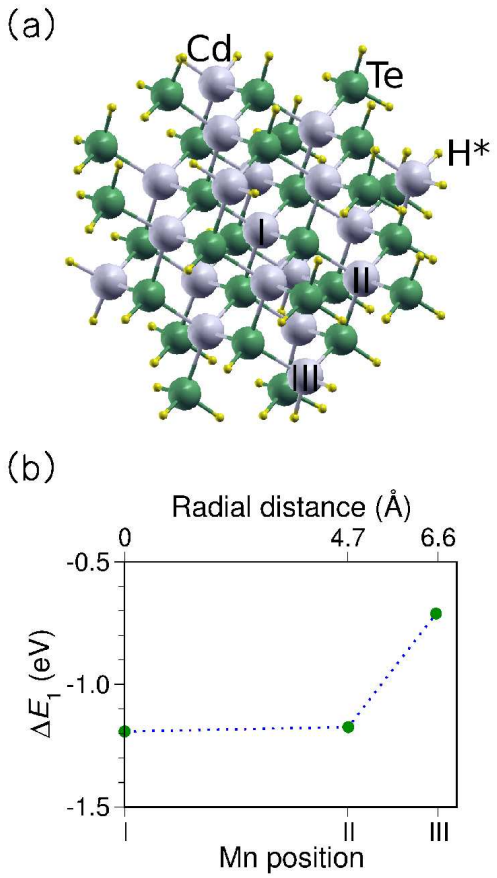

FIG. 1: (Color online) (a) Nanoparticle of (Cd,Mn)Te with 107 atoms: Cd atoms with light gray, Te atoms with dark gray (green) and passivating H* atoms with small spheres. The cation sites are distributed in three groups; labelled as "I" for the center, "II" for inner atoms and "III" for nearest neighbors to surface atoms. (b) Substitutional energy ΔE_1 for a single Mn impurity. We are referring to the ions in solution. The higher is the energy the more stable is the Mn atom in such position.

Due to the preparation of NCs in solution, we take as source systems for Mn and Cd their respective ions. The substitutional energies are shown in Fig. 1 (b) for the positions I, II, and III. All the energies are endothermic. This means that the synthesis of these NCs requires high temperatures as shown in experiments[11]. The changes in ΔE_1 show opposite trends to the QD calculated total energies as a function of Mn site. The lowest-energy sites belong to group III with Mn atoms close to the surface; the outward sites are the most stable positions for the impurity. This outward stability is consistent with other results for magnetic impurities in other semiconductor nanoscale objects, such as nanowires[35].

In the output geometry, the nearest-neighbor distances to the Mn impurity are about 2 % smaller than the Cd-Te distance for the undoped NC. This contraction effect depends strongly on the exchange-correlation approach. The neighbor Mn-Cd distances at the GGA level contract by more than 4 % respect to the bulk Cd-Te distance. However, when relaxing the geometries with the $+U$ scheme the distances expand closer to the unrelaxed input Cd-Te distances. This result could justify the use of unrelaxed Cd-Te distances in other works about Mn doping, but in principle this agreement seems fortuitous.

B. Magnetism and Electronic Properties

We analyze next the origin of magnetism as we are dealing with Mn, that typically is a magnetic element. The total magnetic moment associated with the QD is 5 μ_B, as expected since the Mn dopant introduces five spin-up electrons. The local magnetic moment in Mn impurity is nevertheless smaller, 4.65 μ_B. It differs substantially from the bulk value, 4.21 μ_B, for Mn in bulk CdTe as given in a recent work[27]. The spin density is spatially plotted in Fig. 2. The negative areas of spin density in the Mn nearest-neighbor Te sites integrate to small magnetic moments about $-0.01\,\mu_B$. Such Te atoms were non-magnetic before doping. Other radii for the integration spheres different from the default Wigner-Seitz radii change only slightly these local magnetic moment values. Note that the $+U$ approach affects the charge distribution and thus modify the local moment on Te, which changes in sign when improving the d-level description. This behavior is in disagreement with other previous results concerning CdTe:Mn bulk[27], where the Te and Mn moments are found to be parallel. The Mn magnetic moment is lower than 5 μ_B because of the sp-d hybridization between the localized $3d$ electrons of Mn impurity and the delocalized s- and p-type valence states of CdTe host.

Before studying the sp-d hybridization, lets comment the gaps using the local density of states (DOS) as given in Fig. 3. Quantum confinement in QDs produces a blue shift of the gap and all the related optical properties, such as excitons. The gaps calculated using LDA or GGA approximations are well known to underestimate the experimental values. The calculated gap of CdTe bulk is 0.69 eV which is lower than in experiments, 1.48 eV. Our calculated HOMO-LUMO gap in the Cd-Te QD is 2.59 eV, which shows the predicted blue shift. All these findings are well established in semiconductor QDs. However, the HOMO-LUMO gap of the CdTe dot doped with Mn and within the $+U$ approach remains almost constant to 2.62 eV [see Fig. 3 (a)] when Mn is in the center. We note that the GGA approach understimates the gap and becomes 2.04 eV. Moving Mn to other positions changes this gap value within a tenth of eV, which is negligible to be commented [see Fig. 3 (b)].

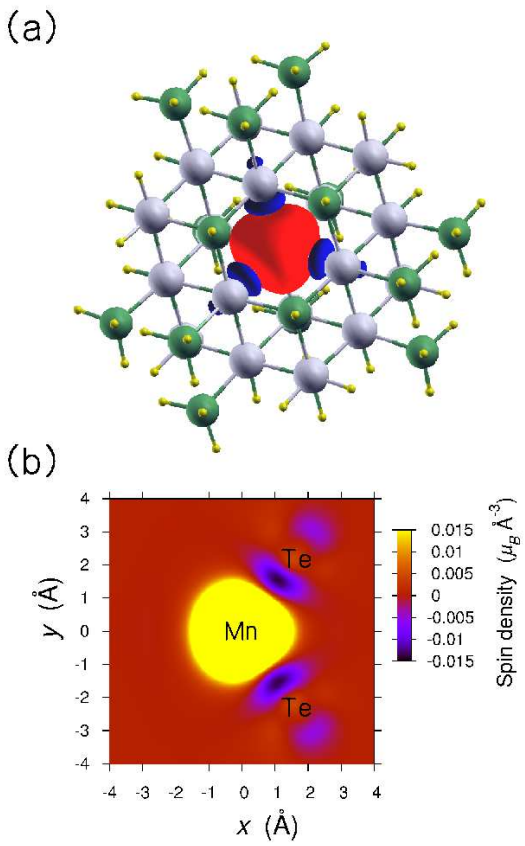

FIG. 2: (Color online) (a) Spin-polarization isosurfaces when the Mn impurity is placed at the center for cuts at ±0.01 μ_B/ Å^3. Positive values are light gray (red); negative values, dark gray (blue). (b) Spin density in a plane defined by the central Mn impurity and two nearest-neighbor Te atoms. For the sake of clarity, spin-up density is chopped at 0.015 μ_B Å^{-3}. The spin-down density region yields on the Te sites a magnetic moment of -0.01 μ_B, antiferromagnetically coupled to the Mn magnetic moment (4.65 μ_B).

1. *Origin of Mn QD-Exchange Coupling*

The *sp-d* hybridization is studied using the local density of states (LDOS) projected into the orbitals of Mn impurity and of nearest-neighbor Te atoms. The main peak of Mn *d*-states appears below the *p* part valence band. Due to the tetrahedral symmetry in CdTe lattice, the five spin-up Mn electrons are split into a triplet of t_2 symmetry and a doublet of e symmetry. We are interested in the magnetic coupling between Mn and NC states equivalent to the band-edge states. The projected DOS around valence- and conduction-edge states are shown in Fig. 3. The conduction-edge states of the host compound show *s*-type character and do not hybridize with the $3d$ orbitals of central Mn, or hybridize sligthly for off-center Mn. Hence, the *s-d* exchange interaction arises mainly from Coulomb repulsion and the Pauli exclusion principle[7,9,15], and originates the spin splitting of these states. This splitting is thus always ferromagnetic, and its exchange constant $N_0\alpha$ is positive. On the contrary, the valence band-edge states of the CdTe are *p*-type and allowed to hybridize fully with the Mn $3d$ orbitals. Anyhow such *p-d* hybridization is small and yields an effective exchange mechanism of interaction between Mn atoms[25]. This exchange is related to the opposite polarization between the valence band-edge states and the Mn $3d$ orbitals. The *p-d* interaction originates the spin splitting of valence-band edge and it is always antiferromagnetic, since all the $3d$ spin-up states are occupied and only jumps into the $3d$ spin-down states are available. The corresponding exchange parameter $N_0\beta$ is thus always negative.

2. *Site Dependence of the Exchange Constants*

Now we compute the *sp-d* exchange interaction parameters $N_0\alpha$ and $N_0\beta$ following the expressions for bulks. They are defined in the standard mean-field theory as[7,20,25,27,36,37]

$$N_0\alpha = \frac{\triangle E^c}{x\langle S_z\rangle}, \text{ and } N_0\beta = \frac{\triangle E^v}{x\langle S_z\rangle}. \qquad (2)$$

The number N_0 is the cations per unit volume[23]. The differences $\triangle E^{c,v} = E^{c,v}$(spin down) - $E^{c,v}$(spin up) are the spin splittings of the conduction (c)- and valence (v)-band edges. They can be extracted from the density of states depicted in Fig. 3. The x value is the fractional dopant concentration[38], and $\langle S_z\rangle = \frac{5}{2}$ is the average z component of Mn spins.

Following eqn (2) we calculate $N_0\alpha$ and $N_0\beta$ as a function of the impurity position. They are shown in Fig. 4. When the Mn atom occupies the NC center, $N_0\alpha = 0.41$ eV, $N_0\beta = -0.62$ eV and $N_0(\alpha - \beta) = 1.03$ eV. The dopant concentration is $x = 1/19 \sim 0.05$ and these values are comparable with the experimental ones obtained for bulk $Cd_{0.95}Mn_{0.05}Te$: $N_0\alpha = 0.22$ eV, $N_0\beta = -0.88$ eV and $N_0(\alpha - \beta) = 1.10$ eV[25]. For NCs, the absolute values of $N_0\beta$ and $N_0\alpha$ are close to each other. When the impurity is located off-center, the exchange constants are smaller than the bulk values and they tend to zero as the impurity approaches the surface. This finding is explained because the Mn bond is expected to be less covalent when Mn is located near the surface, where it is less bulk-like. This site dependence of the exchange constants seems to have implications for random distribution of NCs. When there is a collection of QDs, and each containing a single Mn impurity randomly placed, the average $N_0(\alpha - \beta)$ would be significantly reduced in comparison with the bulk intrinsic Zeeman splitting. This decrease fits in the previous theoretical results[10,19]. The decrease of the exchange splitting is correlated with a smaller CdTe dot density around Mn. Thus, a further density analysis of band-edge states will be needed.

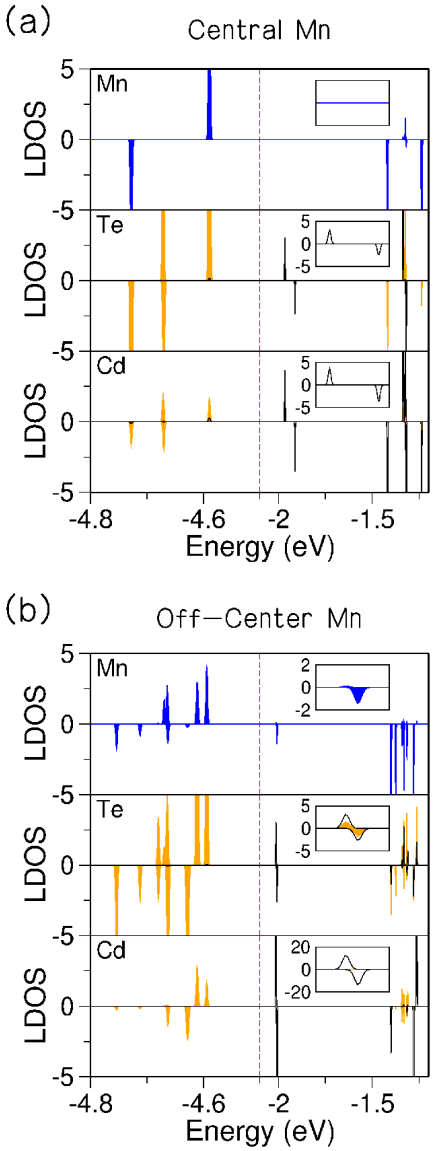

FIG. 3: (Color online) Projected DOS in Mn impurity, d-type, and in the nearst-neighbor atoms Cd and Te, s-type in black (black) and p-type in gray (orange). In panel (a) Mn is placed at the QD center; and panel (b), Mn at site II. Insets widen the conduction edge states. The dashed vertical lines separate the edges of valence band and conduction band.

3. *Densities of HOMO-LUMO States, in and off-Center Positions*

Though the detailed wavefunctions, as we have seen, are not required in the study of exchange interaction parameters, we must clearly attribute them to the electron and the hole effective states which reflect the character of the conduction and valence states in the NCs doped with Mn. Our idea is to look at the High Occupied Molecular Orbital (HOMO) as a representation for the hole; and at the Lowest Unoccupied Molecular Orbitals (LUMO), for the electron. They are shown in Figs. 5 and 6.

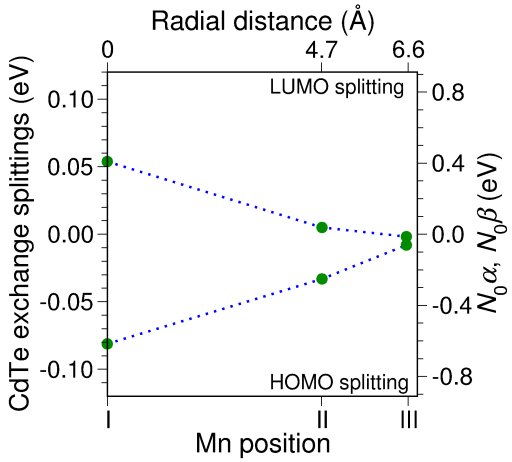

FIG. 4: (Color online) Exchange splitting of band edges (left) and the $N_0\alpha$ and $N_0\beta$ exchange constants (right) as a function of the position (below) and the distance (above) between the impurity and the NC center. Positive values are LUMO splittings; and negative values, HOMO splittings.

We do not include here the HOMO-LUMO states of the undoped NC because they are indistinguishable by simple eye inspection from the up wavefunction in Fig. 5 (a) and (c) for Mn in the dot center. The main contribution to the up HOMO comes from the nearest-neighbor Te atoms and is larger than from any other Te atom. Although more delocalized, the up LUMO has larger contributions in the Cd atoms and in the center site, which is Mn or Cd for doped or undoped dots respectively. These spatial distributions reflect the Te and Mn local DOS character for the HOMO and LUMO commented in the previous sections.

However, the HOMO and LUMO down states are different from the undoped NCs . For the down states we see that the Mn placed in the center expels charge, which is quantified by integrating it around the sphere center in Figs. 5 (e) and (f). This effect is much larger for the HOMO than for the LUMO, see insets. This difference can be explained partially because the HOMO state is occupied, and mainly because the LUMO state does not hybridize with the Mn states, as shown in the previous DOS plot [Fig. 3], which means that it has lower interaction with the d-electrons of Mn. The down HOMO state undergoes the strongest change in comparison with its undoped counterpart because the undoped HOMO is mainly in the nearest-neighbor Te to the central Mn, with which the Mn must couple antiferromagnetically.

To end this section we comment the density of the HOMO and LUMO states for off-center Mn. They are plotted for the position II in Fig. 6. There is larger mixing in the LUMOs which makes that both up and down states remove charge from the Mn neighborhood. The general form of the rest of the LUMOs resembles those of the sphere without Mn. The HOMOs with off-center Mn suffer larger differences with respect to the undoped case, specially for the down component. Anyhow, we see

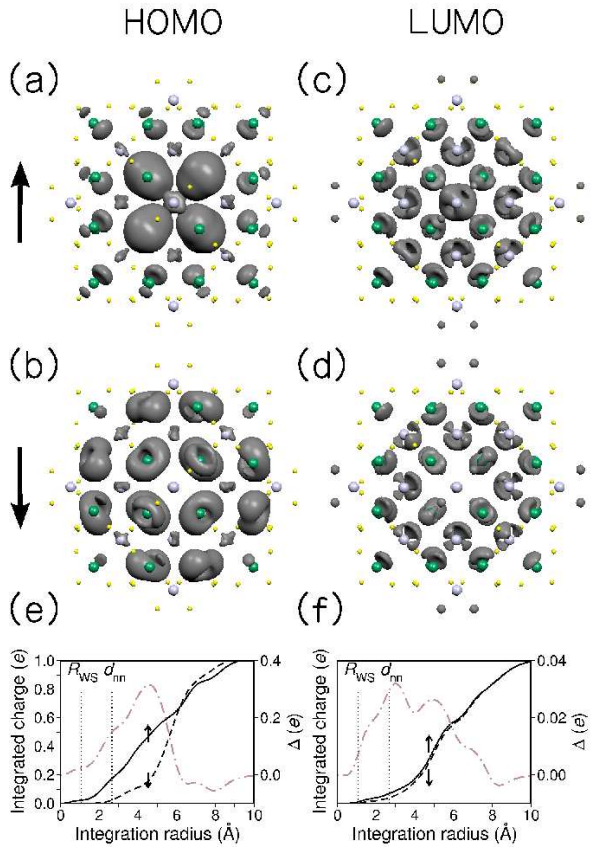

FIG. 5: (Color online) Orbital densities in the Mn-centered sphere for the Highest Occupied Molecular Orbital (HOMO): (a) and (b) for up and down states. Also the densities for the Lowest Unoccupied Molecular Orbital are shown in (c) and (d) panels, up and down respectively. The density cut is around one third of the maximum value. The integrated charges around nanoparticle centers are given in (e) and (f) for HOMOs and LUMOs, respectively. Their up-down differences are plotted as dashed-dotted lines in gray. The Cd Wigner-Seitz Radius $R_{\rm WS}$ and the nearest-neighbor distance $d_{\rm nn}$ are also shown with vertical dotted lines.

a depletion of charge around central Mn mainly for the down part. These larger differences for the HOMO are due to two reasons: (i) the stronger mixing of states in a structure with lower symmetry for Mn off-center, and (ii) the small value for the undoped charge density out of the dot center. The latter means that when Mn is off-center, the states can suffer naturally stronger perturbations. Such is the case for the HOMO-LUMO states with off-center Mn. They show larger voids or lower values of the density around Mn.

C. Analysis of Valence-Band Edge States and Occupied Mn Levels

Exchange splitting of the conduction edge states has been discussed at some length in the previous sections. Here, we look again at the splitting of the valence-band

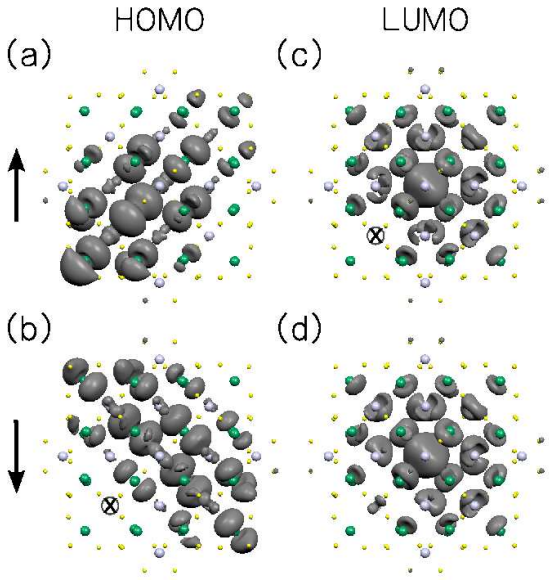

FIG. 6: (Color online) HOMO-LUMO densities for Mn off-center in position II. Panels (a)-(d) are organized as in the previous figure. The crossed atom denotes Mn.

border by looking at the nearest border states. This analysis is useful to clarify the breaking of symmetry in CdTe levels and Mn d levels due to the Mn displacement from the central position.

The valence edge states for Mn in position I are shown with empty dashes in Fig. 7 (a) for up and down spins. The states are three-fold degenerate and we have commented at some length about their characteristics in the previous section. In this panel we show also the valence edge states for Mn in position II along the x direction of displacement. The off-center Mn breaks the degeneracy of these three states. We have identified the global characteristics of these states, although sometimes they have a strong mixed character. The P_y and P_z orbitals, perpendicular to Mn shift, have a smaller splitting. The global P_x suffers the largest splitting as it is parallel to the Mn displacement direction. These electronic levels for Mn in position II explain naturally why the spin splitting of up-down valence band edges is reduced to half value, respect to Mn at the center.

These splittings are correlated to those of Mn levels, plotted in Fig. 7 (b). For central Mn the occupied d levels are grouped in two sets: the first has $d_{x'^2-y'^2}$ and $d_{z'^2}$, the second gets the cross d levels $x'y'$, $y'z'$, and $z'x'$. These cross orbitals have lower energy which is typical for a Cd vacancy Va_{Cd} interacting with the tetrahedrally split $Mn-d$ electrons [see branching scheme in Fig. 8]. The removal of a Cd atom creates a vacancy Va_{Cd}. The t_2 levels of the Va_{Cd} hybridize with the t_2 states of Mn atom and produce the bonding t_2^b and antibonding t_2^a states. As the Mn states are very low in energy the t_2^b states resembles much the $Mn-t_2$ states and cross over

the $Mn-e$ states. While the t_2^a states remain close to the QD semiconductor states. For Mn in position II, the d levels shift upwards in energy, typical for the smaller CdTe density around Mn, as seen in the section about site dependence of exchange constants. The e levels remain degenerate. The t_2^b states ($x'y'$, $y'z'$, and $z'x'$) split although they still are groupable together. The orbital $z'x'$ orthogonal to the Mn displacement has the highest energy. The orbitals $x'y'$ and $y'z'$ remain at lower energy, the lowest energy for the $x'y'$ orbital with the lobes in the Mn displacement direction from the center.

We want to stress finally that the Mn has a much larger exchange splitting of several eV that polarizes the CdTe levels in much smaller amount, in the order of several hundredths of eV. This spin polarization of CdTe in NCs depends on the Mn position. Although the splitting of CdTe levels that interact strongly with Mn is almost independent of position (P_x), the other levels (P_y and P_z) remain almost unaffected. This finding means that the exchange splitting of the up-down CdTe valence edge amounts to nearly less than half of the value with central Mn.

IV. NANOCRYSTALS WITH TWO MN IMPURITIES

We investigate (Cd,Mn)Te NCs doped with two Mn impurities. The substitutional energy differences ΔE_2 are calculated for the following reaction:

$$\text{CdTe NC} + 2\text{Mn}^{+2} \longrightarrow \text{CdTe:Mn NC} + 2\text{Cd}^{+2}. \quad (3)$$

The calculated differences against the Mn positions and the distance between Mn atoms are displayed in Fig. 9. When both Mn impurities occupy sites I-II and II-II, the energies ΔE_2 are larger than for positions I-III and II-III. This difference is about 0.5 eV. The substitutional energy of Cd decreases with the presence of Mn atoms at surface sites III. This trend follows the previous energy differences ΔE_1 for a single Mn in Fig. 1, where position III is the most stable. The interaction energy is the difference between the previous ΔE_2 Mn-Mn energy and the sum of single Mn energies ΔE_1 in the NC. We plot also the interaction energy (Δ) between the two Mn impurities in Fig. 9 (b). The changes of the interaction energy Δ due to Mn positions are an order of magnitude lower than those of the substitutional energy ΔE_2. The interaction Δ is 32 meV for Mn-Mn atoms in sites I-II and 21 meV in III-III. It seems that the closer the Mn impurities the larger their interaction energy. However, the dependence of Δ with the distance between the two Mn impurities is almost flat except when Mn atoms are next-nearest neighbors or close to the surface.

To a lesser extent these energies ΔE_2 and Δ also depend on the magnetic configuration between Mn magnetic moments. We consider two magnetic coupling cases for Mn moments: ferromagnetic in which $\mu_{QD} = 10\ \mu_B$,

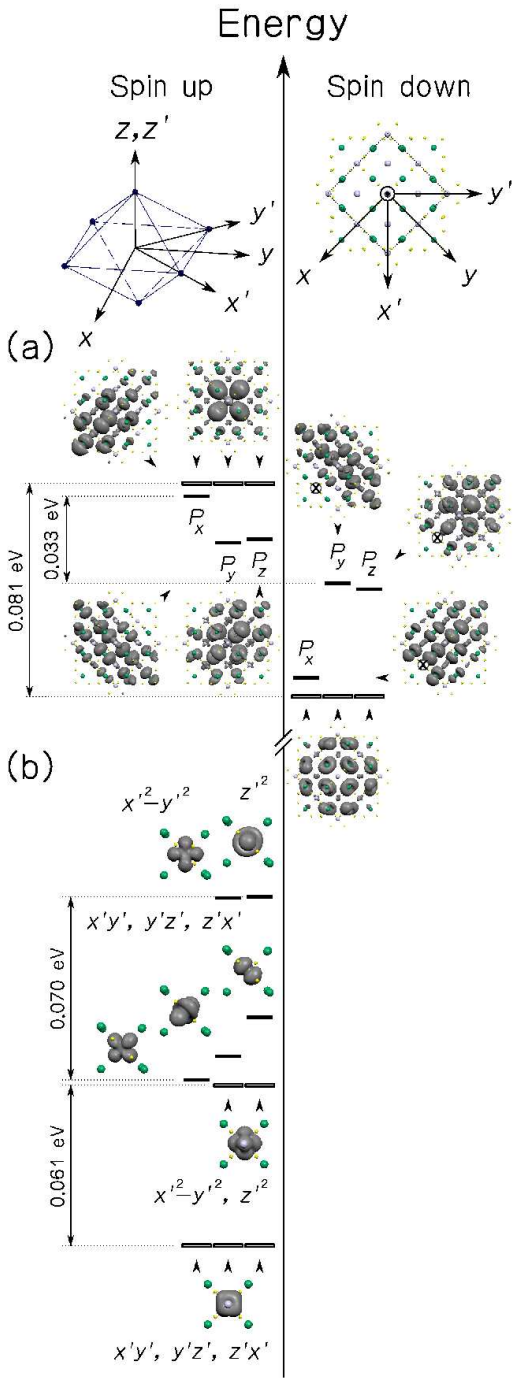

FIG. 7: (Color online) (a) Valence states close to the Fermi energy for Mn in center with empty lines; and for Mn off-center in position II with full lines. The global densities are given nearest to the corresponding states. The notation concerning atom labeling and density cuts follows the one given in previous figures. The geometrical insets show the reference systems. The degeneracy gets lower for the off-center position, however the quantum dot states P_y and P_z are nearly degenerate. (b) Mn d states for center and off-center position. We see the splitting between the triplet t_2 and doublet e states [see next figure for their order explanation].

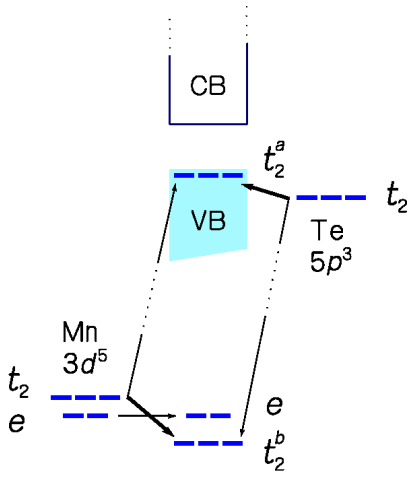

FIG. 8: (Color online) Branching diagram for a substitutional Mn atom in CdTe dot. The states of substitutional Mn atom (center) are originated in the hybridization of vacant Cd states $Va_{Cd} - t_2$ (right) with Mn-d states (left).

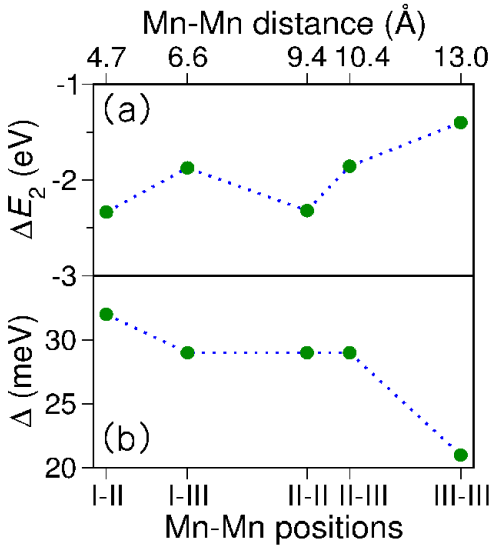

FIG. 9: (Color online) (a) Substitutional energy of two Mn positions. (b) Interaction energy Δ for various Mn-Mn pairs. It shows the difference between the previous total Mn-Mn energy and the sum of single Mn energies in the NC.

and antiferromagnetic in which $\mu_{QD} = 0\ \mu_B$. Independently of the Mn positions within the QD, the Mn magnetic moments in the lowest-energy state are coupled antiferromagnetically. This is shown in Fig. 10 using the d-d exchange constant for various Mn-Mn positions instead of the FM-AFM energy differences. In fact, we calculate the d-d exchange constant from the FM-AFM energy differences for various Mn-Mn positions. These constants J^{dd} are depicted in Fig. 10 (a). The largest value in modulus is roughly 1.5 K for Mn atoms on sites I and II. It is about four times smaller than the absolute value of the experimental exchange constant in bulk $Cd_{0.95}Mn_{0.05}Te$, 6.1 K. In addition we can see the dependence with the Mn-Mn sites. For Mn-Mn intermediate distances, the exchange constants decrease even further and they are following the AFM-FM splitting. Note that for the Mn atoms in the center and surface positions this splitting seems to be very small.

We have also examined the d-levels for several of these Mn-Mn configurations, although they are not given here. Due to symmetry in QDs, the d-levels in position I and II are close, but in different energy panels [as seen in previous Fig. 7]. This means that the symmetry considerations are more relevant in QDs to understand the Mn-Mn interaction that higher-order mechanisms, such as superexchange or double exchange. We must remember that such mechanisms are important for DMS bulks where the d-levels are at the same energies, due the equal density around Mn atoms. These symmetry considerations and the smaller dot density around Mn atoms explain the lower coupling J^{dd} constants.

The $N_0\alpha$ and $N_0\beta$ exchange constants are shown in Fig. 10 (b). They are calculated for the ferromagnetic (circles) and antiferromagnetic (squares) states for several Mn-Mn positions; the dopant concentration is $x = 2/19 \sim 0.1$. As in the previous section, the exchange constants get closer to the bulk experimental values when one of the Mn impurities occupies the NC center (I-II and I-III), and they tend to zero when the Mn ions separate from each other and approach the surface. The exchange constants for antiferromagnetic cases with high symmetry are also zero because the down and the up electrons are fully degenerated. When comparing Fig. 4 with Fig. 10, we conclude that the largest exchange values are obtained for NCs doped only with a Mn impurity in the central site. The relative orientation of $N_0\alpha$ and $N_0\beta$ is the same as before. However their values decrease by at least 0.2 eV. This difference can be ascribed to the second Mn atom that cancels partially the coupling to the conduction and valence bands in the neighborhood of the first Mn.

A. Valence Edge States

The valence states around the edges allow us, like in the case of a single Mn impurity analysis, to understand the origin of the exchange in the CdTe states. As it has been done before, they are plotted for the asymmetric Mn-Mn configuration I-II in Fig. 11 and for the symmetric one II-II in Fig. 12. However, due to magnetic coupling there are more options than in one Mn impurity case. Thus the panels (a) denote the FM Mn alignments; and the panels (b), the AFMs.

We shall see that for the results of both figures, a perturbation theory of the central Mn case rationalizes also the level breaking as due to symmetry and magnetic configuration. We therefore start the discussion by consid-

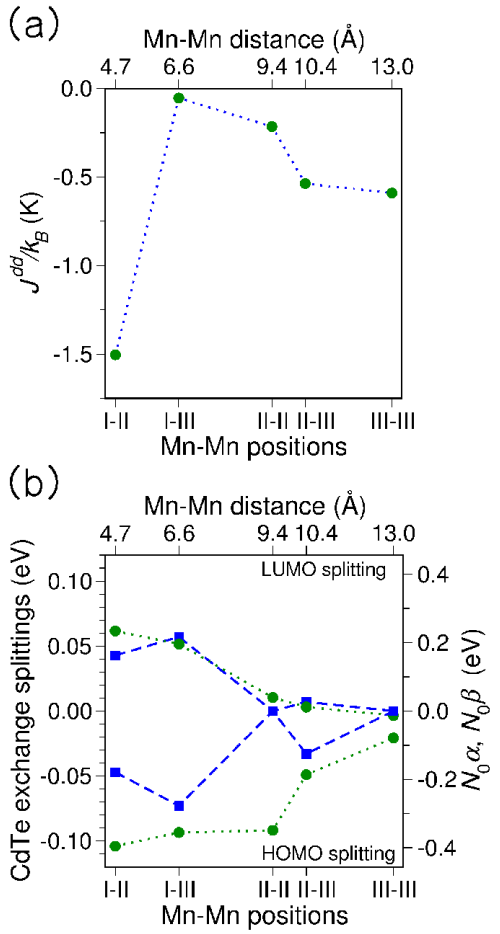

FIG. 10: (Color online) The (a) *d-d* exchange constant together with the (b) *sp-d* exchange constants ($N_0\alpha$ and $N_0\beta$) for several Mn-Mn positions. The J^{dd} are given in K to compare with the bibliography. Exchange splittings follow the notation of Fig. 4: Circle marks with dotted lines (green) denote FM alignments; and square marks with dashed lines (blue), AFM alignments.

ering the AFM case I-II in Fig. 11 (b).

We see that the exchange splitting of the CdTe aligns with the Mn in position I. Let us consider that a Mn in position II perturbs the levels to first order, as in previous one Mn impurity. Now, we can focus on the change in splitting of the three-fold degenerate levels using the previous results. In this way, the down CdTe valence-band edge levels are P_x at low energy, and nearly degenerate P_y and P_z at higher energies. For the up levels this order is reversed. This order is also followed by our computations. The expected and calculated levels are in excellent agreement and thus confirm that a perturbative approach applies to the splitting of CdTe levels by central Mn.

However, the case AFM I-II we have discussed, in which the perturbative approach can be applied, is not the only case of physical interest. In the FM case, Fig. 11 (a) for example, both Mn reinforce their splitting of the CdTe states. The value is close to the sum of both I and II splittings for the Mn impurities on their own. We shall not go into further detail here.

For the case II-II we only draw attention to the fact that there is strong interaction for one up Mn impurity with the CdTe down states. We can see the empty space of up (down) orbitals around the down (up) Mn in Fig. 12 (b) as it expels the surrounding charge. We want to stress here that for the FM case in Fig. 12 (a) we need to go beyond the previous simple perturbative analysis. In spite of the strong perturbation, it means that it is more difficult to interpret the data as coming from a perturbation due to a second impurity. It remains true that there is a clear increase of the splitting of P_x orbital aligned along the corresponding Mn-Mn direction.

V. CONCLUSIONS

In summary, we have investigated the electronic and magnetic properties of (Cd,Mn)Te nanocrystals of spherical shape with the density functional theory. The embedded Mn impurities substitute Cd atoms in the zinc blende lattice. The QDs are $\sim$ 2 nm in diameter, centered on a cation site (Cd), and they have a total of 107 atoms. The Cd and Te dangling bonds on the surface are passivated by pseudohydrogen atoms (H*), which are the simplest model for a real organic ligand. We have studied two doping situations: NCs including one and two Mn impurities.

In the first case we find that the configuration with the Mn atom near the surface presents the lowest energy. The Mn impurity introduces five *d*-type spin-up electrons within the NC, thus the total magnetic moment associated with the QD is 5 μ_B, as expected. The local Mn magnetic moment is 4.65 μ_B. It is smaller than 5 μ_B because of the *s,p-d* hybridization. Also the Mn-nearest-neighbor Te sites show small magnetic moments antiferromagnetically coupled to the Mn moment. Furthermore, we look at the hybridization in the density of states. We calculate the *sp-d* exchange constants for various Mn locations. The exchange constants are comparable to the bulk ones when the impurity is at the center, and they go to zero when the Mn is close to the NC surface. Then, for central Mn we introduce spatially the HOMO and LUMO states to verify that the largest change is for the down HOMO, which also justifies the antiferromagnetic alignment of the nearest-neighbor Te atoms. Additionally, we check the role of symmetry by looking at the CdTe levels near the valence-band edge. This allows us a clear interpretation of the origin of exchange splitting. The P_x levels in the Mn diplacement direction suffer the stronger hybridizaton, while the P_y and P_z levels remain almost unsplit. Thus, the exchange contants are roughly half of the central Mn case.

In the second case we calculate the total ground-state energy as a function of Mn-Mn positions and the magnetic configuration of their local magnetic moments. In the minimum-energy state the Mn dopants are on the

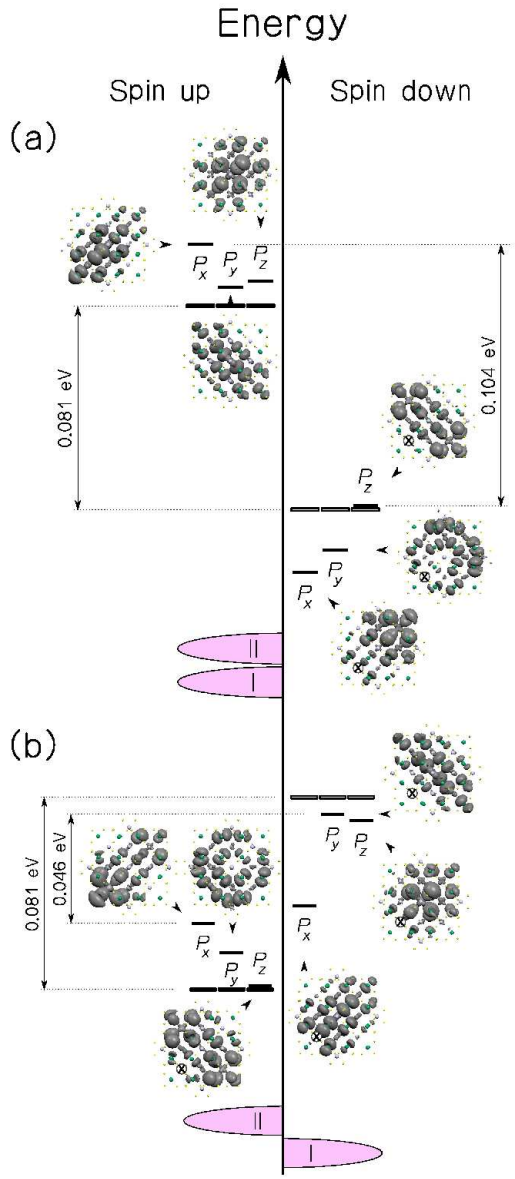

FIG. 11: (Color online) Valence states closest to the Fermi energy for Mn in configuration I-II with full lines for (a) FM and for (b) AFM couplings. The empty dashes refer to a previous case with Mn in a central position. The global densities are given nearest the corresponding states. The notation concerning atom labeling and density cuts follows the one given in previous figures. At the bottom, a scheme of Mn magnetic moments is shown. For the ground AFM case the valence states split according to center Mn in position I, however the degeneracy follows closely the off-center Mn in position II.

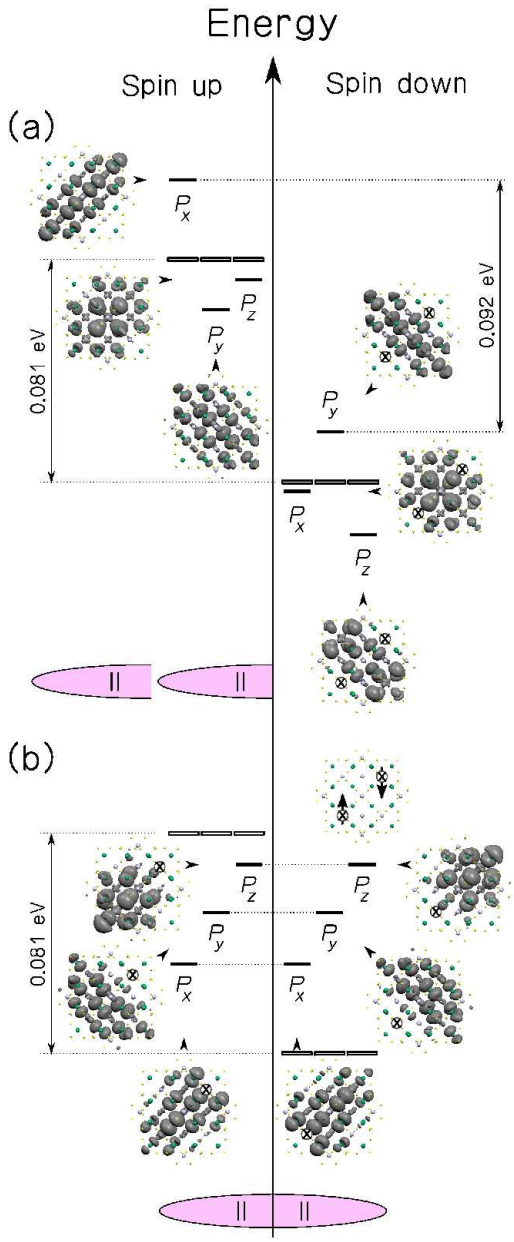

FIG. 12: (Color online) Valence states closest to the Fermi energy for Mn in symmetric configuration II-II with full dashes for (a) FM and for (b) AFM couplings. They follow the notation of the previous figure. For off-center positions the valence states break the degeneracy even further.

surface, as far apart as possible, and antiferromagnetically coupled. We calculate the *sp-d* and *d-d* exchange constants for various Mn-Mn locations. We find that the exchange constants $N_0\alpha$ and $N_0\beta$ are comparable to the corresponding bulk values when impurities occupy central bulk-like positions (I-II). They tend to zero as they separate from each other or approach the surface. As for the exchange $|J^{dd}|$, its largest value is for the Mn ions placed in central bulk-like sites (I-II), and is four times smaller than in the bulk with similar Mn concentration. A similar analysis of states nearest the valence-band edge demonstrates that a perturbative approach seems to be valid, with exception of the II-II FM configuration.

Acknowledgments

This work was supported by the Basque Government through the NANOMATERIALS project (IE05-151) under the ETORTEK Program (NANOMAT), Spanish Ministerio de Ciencia y Tecnología (MCyT) of Spain (Grant No. Fis 2004-06490-CO3-00 and MONACEM project) and the European Network of Excellence NANOQUANTA (NM4-CT-2004-500198). The computing resources from the Donostia International Physics Center (DIPC) are gratefully acknowledged. Prof. A. K. Bhattacharjee is acknowledged for comments on the manuscript. Carlos E.-A. wants to thank N. González for support on the plotting routines during this work.

[1] Y. Wang and N. Herron, Physical Review B **42**, 7253 (1990).
[2] Y. Wang and N. Herron, J. Phys. Chem. **95**, 525 (1991).
[3] V. Albe, C. Jouanin, and D. Bertho, Physical Review B **58**, 4713 (1998).
[4] J. Pérez-Conde and A. K. Bhattacharjee, Solid State Communications **110**, 259 (1999).
[5] S. Sapra and D. D. Sarma, Physical Review B **69**, 125304 (2004).
[6] V. Albe, C. Jouanin, and D. Bertho, Physical Review B **57**, 8778 (1998).
[7] A. K. Bhattacharjee, G. Fishman, and B. Coqblin, Physica B+C **117-118**, 449 (1983).
[8] R. N. Bhargava, D. Gallagher, X. Hong, and A. Nurmikko, Physical Review Letters **72**, 416 (1994).
[9] A. K. Bhattacharjee, Physical Review B **49**, 13987 (1994).
[10] A. K. Bhattacharjee, Physical Review B **51**, 9912 (1995).
[11] D. J. Norris, N. Yao, F. T. Charnock, and T. A. Kennedy, Nano Letters **1**, 3 (2001).
[12] D. V. Melnikov and J. R. Chelikowsky, Physical Review Letters **92**, 046802 (2004).
[13] S. C. Erwin, L. J. Zu, M. I. Haftel, A. L. Efros, T. A. Kennedy, and D. J. Norris, Nature **436**, 91 (2005).
[14] S. A. Wolf, D. D. Awschalom, R. A. Buhrman, J. M. Daughton, S. von Molnar, M. L. Roukes, A. Y. Chtchelkanova, and D. M. Treger, Science **294**, 1488 (2001).
[15] J. Szczytko, W. Mac, A. Twardowski, F. Matsukura, and H. Ohno, Physical Review B **59**, 12935 (1999).
[16] D. M. Hoffman, B. K. Meyer, A. I. Ekimov, I. A. Merkulov, A. L. Efros, M. Rosen, G. Couino, T. Gacoin, and J. P. Boilot, Solid State Communications **114**, 547 (2000).
[17] K. Yanata, K. Suzuki, and Y. Oka, Journal of Applied Physics **73**, 4595 (1993).
[18] A. K. Bhattacharjee, Physical Review B **58**, 15660 (1998).
[19] I. A. Merkulov, D. R. Yakovlev, A. Keller, W. Ossau, J. Geurts, A. Waag, G. Landwehr, G. Karczewski, T. Wojtowicz, and J. Kossut, Physical Review Letters **83**, 1431 (1999).
[20] N. S. Norberg and D. R. Gamelin, Journal of Applied Physics **99**, 08M104 (2006).
[21] T. A. Kennedy, E. R. Glaser, P. B. Klein, and R. N. Bhargava, Physical Review B **52**, R14356 (1995).
[22] L. Besombes, Y. Leger, L. Maingault, D. Ferrand, H. Mariette, and J. Cibert, Physical Review Letters **93**, 207403 (2004).
[23] A. K. Bhattacharjee and J. Pérez-Conde, Physical Review B **68**, 045303 (2003).
[24] N. Q. Huong and J. L. Birman, Physical Review B **69**, 085321 (2004).
[25] B. E. Larson, K. C. Hass, H. Ehrenreich, and A. E. Carlsson, Physical Review B **37**, 4137 (1988).
[26] J. P. Lascaray, D. Coquillat, J. Deportes, and A. K. Bhattacharjee, Physical Review B **38**, 7602 (1988).
[27] A. E. Merad, M. B. Kanoun, and S. Goumri-Said, Journal of Magnetism and Magnetic Materials **302**, 536 (2006).
[28] G. Kresse and J. Hafner, Physical Review B **47**, R558 (1993).
[29] G. Kresse and J. Furthmüller, Physical Review B **54**, 11169 (1996).
[30] G. Kresse and D. Joubert, Physical Review B **59**, 1758 (1999).
[31] J. P. Perdew, K. Burke, and M. Ernzerhof, Physical Review Letters **77**, 3865 (1996).
[32] I. V. Solovyev and P. H. Dederichs, Physical Review B **49**, 6736 (1994).
[33] S. J. Youn, B. I. Min, and A. J. Freeman, Physica Status Solidi B **241**, 1411 (2004).
[34] X. Huang, E. Lindgren, and J. R. Chelikowsky, Physical Review B **71**, 165328 (2005).
[35] T. M. Schmidt, P. Venezuela, J. T. Arantes, and A. Fazzio, Physical Review B **73**, 235330 (2006).
[36] H. Raebiger, A. Ayuela, and R. M. Nieminen, J. Phys.: Condens. Matter **16**, L457 (2004).
[37] H. Raebiger, A. Ayuela, and J. von Boehm, Physical Review B **72**, 014465 (2005).
[38] J. M. Fatah, T. Piorek, P. Harrison, T. Stirner, and W. E. Hagston, Physical Review B **49**, 10341 (1994).